9

10

11

12

13

14

15

16

17

18

19 20

21

22

23

24

25

26

27

28

29

30

31

32

33

34 35

36

37

38

39

42

43

44

45

46

47

48

49

50

51

52

53

54

55

56

57

58

59

60

61

62

63

64

65

66

Physics Letters A ••• (••••) •••-•••



Contents lists available at ScienceDirect

Physics Letters A

www.elsevier.com/locate/pla



68

69

70

71

72

73

74

75

76

77

78

79

80

81

82

83

84

89

90

91

92

93

94

95

96

97

98

99 100

101

102

103

104

105

107

108

109

110

111

112

113

114

115

116

117

118

119

120

121

122

123

124

125

126

127

128

129

130

131

132

Nonparaxial Bessel and Bessel-Gauss pincers light-sheets

F.G. Mitri

Chevron, Area 52 Technology - ETC, 5 Bisbee Ct., Santa Fe, NM 87508, United States

ARTICLE INFO

Article history: Received 6 October 2016 Received in revised form 28 October 2016 Accepted 31 October 2016 Available online xxxx Communicated by V.A. Markel

Kevwords: Bending light Angular spectrum decomposition in plane Opto-fluidics Optical tweezers Beam-shape coefficients

ABSTRACT

Nonparaxial optical Bessel and Bessel-Gauss pincers optical-sheets are introduced based upon the angular spectrum decomposition in plane waves. The angular spectrum function and the beam-shape coefficients are expressed by means of improper integrals computed numerically. The radiated component of the electric field is also evaluated, displaying unique features of the nonparaxial Bessel pincers light-sheets. This new type of light-sheets finds potential applications in the development of novel methods in optical light-sheet tweezers for particle manipulation in opto-fluidics, particle sizing and imaging. Numerical predictions for the scattering, radiation force and torque, and particle dynamics also benefit from the developed beam solution.

© 2016 Elsevier B.V. All rights reserved.

Bending the wave field without modification and design of the medium of wave propagation is highly desirable in the development of emergent technologies in optical surface wave tweezers and opto-fluidics applications. One particular example is the nonparaxial Airy light-sheet [1] that has been recently introduced for potential applications in particle manipulation [2] and handling along curved trajectories [3]. Nonetheless, the Airy beam bending angle is relatively weak and there is a need to investigate improved solutions to further achieve larger bending angles, which can be very beneficial for imaging around steep corners, and in particle manipulation applications with minimal hampering by obstacles.

Along that direction of research, the present analysis suggests a novel nonparaxial beam solution, where the electric field has the shape of light-sheet pincers (i.e. slice of a beam in 2D) with tight bending arcs. This beam type is obtained by adequate apodization at the surface of the optical source using the cylindrical Bessel function of integer order m (in addition to the Gaussian function). It is of some importance to investigate novel solutions of beams yet to be explored from the standpoint of optical scattering, radiation force, torque and particle dynamics theories [4,5] for optimal experimental design and the development of new avenues for applications in optical tweezers, particle manipulation and imaging. Notice that the standard 3D Bessel [6-9] and Bessel-Gauss beams [10] possess limited-diffraction properties [11], with the self-healing ability [12,13] as they reform after encountering an obstacle. The characteristics of the 2D solutions developed here differ from the 3D case such curving/bending arcs of maximal electric field magnitude can be synthesized. Moreover, their shapes can be controlled and bent to become quasi-circular depending on the light-sheet beam parameters, which may provide an advantage over the "abruptly autofocusing waves" [14] displaying a radial caustic collapse in the nonparaxial limit [15].

Consider a light-sheet beam in 2D propagating along the x'-direction with invariance with respect to the z'-axis (Fig. 1), with an electric field polarized along the z-direction (i.e. transverse electric TE-polarization such that $E_x^{\text{inc}} = E_y^{\text{inc}} = H_z^{\text{inc}} = 0$). A time variation in the form of $e^{-i\omega t}$ is assumed but suppressed from the equations for convenience.

For the purpose of the present study, the initial beam profile describing the electric at the origin of the beam (x = 0) is chosen

$$E_z^{\text{inc}}(0, y) = E_0 J_m(\alpha k y), \tag{1}$$

where E_0 is the electric field amplitude, $J_m(.)$ is the cylindrical Bessel function of the first kind of integer order m, the parameter k is the wavenumber and $\alpha > 0$ is a scaling (real) parameter.

Based on the angular spectrum decomposition in plane waves [16], the incident electric field component in space E_7^{inc} is expressed in a system of Cartesian coordinate as,

$$E_{z,m}^{\text{inc}}(x,y) = \int_{-\infty}^{+\infty} S_m(p,q)e^{ik(px+qy)}dq,$$
 (2)

E-mail address: F.G.Mitri@ieee.org.

http://dx.doi.org/10.1016/j.physleta.2016.10.055 0375-9601/© 2016 Elsevier B.V. All rights reserved.

68 69

73

75

76

77

78

79

87

95

96

97

98

99

100

101

102

103

104

105

106

107

108

109

110

111

112

113

114

115

116

117

118

119

120

121

122

123

124

125

126

127

128

129

130

131

132

10

12

13

14

15

16 17

18

19

20 21

22

23

24

25

26

27

28

29

30

31

32

33

34

35

36

37

39

40

41

42

43

44

45

46

47

48

49

50

51

52

53

54

55

56

57

58

63

64

65

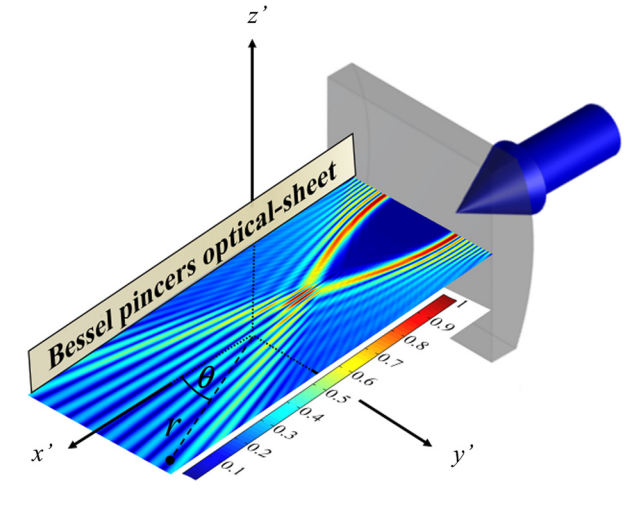


Fig. 1. Graphical representation of the propagation of a nonparaxial optical pincers light-sheet, propagating along the x'-direction with invariance along the z'-axis.

where (p,q) are the directional cosines in polar coordinates such that $p = \cos \chi$, $q = \sin \chi$, and χ is the angle of propagation of the individual plane wave. Notice that Eq. (2) constitutes an exact solution of the Helmholtz and Maxwell's equations. The function $S_m(p,q)$ is known as the angular spectrum which characterizes the initial profile of the beam at the origin x = 0, and is obtained from the inverse Fourier transform.

$$S_m(p,q) = \begin{cases} \left(\frac{k}{2\pi}\right) \int_{-\infty}^{+\infty} E_{z,m}^{\text{inc}}(0,y) e^{-ikqy} dy, & \text{if } p^2 + q^2 = 1, \\ 0, & \text{otherwise} \end{cases}$$
(3)

Substituting Eq. (3) into Eq. (2) using Eq. (1), and manipulating the result, the incident electric field component (in Cartesian coordinates) becomes.

$$E_{z,m}^{\text{inc}}(x,y) = \left(\frac{E_0 k}{2\pi}\right) \int_{-\infty}^{+\infty} \left[\int_{-\infty}^{+\infty} J_m(\alpha k y') e^{-ikqy'} dy'\right] e^{ik(px+qy)} dq.$$
(4)

Since m is an integer number, the angular spectrum function can be further simplified [see Appendix A] such that,

$$S_m(p,q)$$

$$= \left(\frac{E_0 k}{2\pi}\right) \left[\int_{-\infty}^{+\infty} J_m(\alpha k y') e^{-ikqy'} dy'\right]$$

$$= \begin{cases} \frac{E_0 i^{-m}}{\pi \alpha^m \sqrt{\alpha^2 - q^2}} \Re\{(q + i\sqrt{\alpha^2 - q^2})^m\}, & \text{if } |q| \le \alpha, \\ 0, & \text{otherwise.} \end{cases}$$
(5)

In an arbitrary system of coordinates shifted from the center of the beam, the following transformations are used, such that,

$$x = (x' - x_0)\cos\theta_i + (y' - y_0)\sin\theta_i, \tag{6}$$

$$y = -(x' - x_0)\sin\theta_i + (y' - y_0)\cos\theta_i,$$
 (7)

where $x' = r \cos \theta$, $y' = r \sin \theta$, and (r, θ) are the polar coordinates (Fig. 1). The parameters $x_0 = r_0 \cos \theta_0$, $y_0 = r_0 \sin \theta_0$, are the coordinates of the shift from the center of the beam where $r_0 = \sqrt{x_0^2 + y_0^2}$, and $\theta_0 = \tan^{-1}(y_0/x_0)$. The parameter θ_i denotes the angle of incidence with respect to the x-axis of wave propaga-

Using the Jacobi-Anger expansion [17], the incident electric field component given by Eq. (2) is rewritten as a multipole expansion series in cylindrical coordinates as,

$$E_{z,m}^{\rm inc}(r,\theta) = E_0 \sum_{n=-\infty}^{+\infty} b_{n,m} J_n(kr) e^{in\theta}, \tag{8}$$

where the $b_{n,m}$ are the beam-shape coefficients (BSCs) given by,

$$b_{n,m} = i^n e^{-in\theta_i} \int_{-\infty}^{+\infty} f_m(p,q) dq, \tag{9}$$

where,

$$f_m(p,q) = S_m(p,q)e^{-i[n\sin^{-1}(q) + kr_0\cos(\sin^{-1}(q) - \theta_0 + \theta_i)]}.$$
 (10)

Notice that the BSCs given by Eq. (9) can be decomposed into the sum of two coefficients representing the radiated and evanescent fields. Therefore, Eq. (9) becomes,

$$b_{n,m} = b_{n,m}^{\text{rad}} + b_{n,m}^{\text{ev}}, \tag{11}$$

$$b_{n,m}^{\text{rad}} = i^n e^{-in\theta_i} \int_{-1}^{+1} f_m(p,q) dq,$$
 (12)

$$b_{n,m}^{\text{ev}} = i^n e^{-in\theta_i} \left[\int_{-\infty}^{-1} f_m(p,q) dq + \int_{+1}^{+\infty} f_m(p,q) dq \right].$$
 (13)

It is important to note that evanescent waves do not propagate to the far-field and their contribution to the total field is negligible [18–20] as they decay exponentially during propagation away from the source. Therefore, the integral bounds for the incident electric field given by Eq. (2) or Eq. (4) reduce to $\int_{-1}^{+1} (...) dq$. For computations related to the optical scattering, radiation force and torque as well as particle dynamics [4], Eqs. (12) and (13) would be utilized in the generalized theory for optical sheets [4,5], thus, their importance from that theoretical and analytical perspectives.

The numerical analysis is started by developing a MATLAB program to compute the angular spectrum function [given by Eq. (3)] and the resulting radiated field [given by Eq. (4)], with particular emphasis on the scaling parameter α and beam order m. Standard numerical integration using the trapezoidal rule has been performed with a sampling step as small as $\delta q = 2 \times 10^{-4}$ to achieve appropriate convergence.

Panels (a)-(c) of Fig. 2 display the numerical computations for the normalized magnitude of the incident electric field $|E_{z,m}^{inc}/E_0|$ in the dimensionless transverse plane (kx, ky) for $\alpha = 0.5$ and beam topological charge m = 10, 45 and 100, respectively. It is interesting to note the spatial region over which the incident field approaches zero (or in some instances vanishes). This area is delimited by large amplitude "bending arcs" of parabolic shapes from either side of the axis ky = 0 in the form of "pincers". The bending arcs interfere and create a focal spot behind that region. The focal spot magnitude is maximal when m is an even integer number, but vanishes along the axis ky = 0 when m becomes an odd integer number. Thus, the Bessel pincers light-sheet possesses an axial null for odd integer orders. As the order of the beam *m* increases [i.e., panel (b)], the dimensions of the pincers and delimited region increase. As m increases further, the bending arcs no longer interfere as shown in panel (c), so that the focal spot magnitude fades out after it decreases while reaching a threshold determined by the values of α and m. For improved visualization of this effect, Visualization 1 shows the animation related to the variations of the topological charge of the beam for $\alpha = 0.5$.

Download English Version:

https://daneshyari.com/en/article/5496890

Download Persian Version:

https://daneshyari.com/article/5496890

Daneshyari.com